ARTICLE

Reactivity of the superhalogen/superalkali ion encapsulated C_{60} fullerenes

Received 00th January 20xx,
Accepted 00th January 20xx

DOI: 10.1039/x0xx00000x

Gibu George,[a] Anton J. Stasyuk *[a,b] and Miquel Solà *[a]

The Diels-Alder cycloaddition reaction between 1,3-cyclohexadiene and a series of C_{60} fullerenes with encapsulated (super)alkali/(super)halogen species ($Li^+@C_{60}$, $Li_2F^+@C_{60}$, $Cl^-@C_{60}$, and $LiF_2^-@C_{60}$) was explored by means of DFT calculations. Reactivity of the ion encapsulated systems was compared to the parental C_{60} fullerene. Significant enhancement in reactivity was found for cation encapsulated $Li^+/Li_2F^+@C_{60}$ complexes. The cycloadduct formed by $LiF_2^-@C_{60}$ was found to be the most thermodynamically favorable among the studied ones. In contrast, encapsulation of Cl^- anion leads to the disfavor of cycloaddition reaction both kinetically and thermodynamically. Higher activation energy barrier and less stability of the reaction product in the case of $Cl^-@C_{60}$ were associated with higher deformation energies of fullerene cage and smaller interaction energy between the reactants in comparison to the other studied complexes.

Introduction

The discovery of buckminsterfullerene C_{60}, and it's La encapsulated derivative marked the beginning of a new era in the field of carbon materials.[1] Since then the endohedral metallofullerenes (EMFs) in which metal atoms, ions, or clusters are incorporated inside a fullerene cage have attracted significant attention from scientists from various fields of science.[2-8] Up today, a huge number of different fullerenes with encapsulated alkali and alkaline metals,[9-11] transition metals,[12,13] lanthanides,[11,14] and neutral species[15-21] have been reported. The unusual behavior of such EMFs in comparison with empty fullerenes resulted in numerous practical applications of EMFs in nanomaterials, bioscience, organic photovoltaics, and others.[22-27,8] The functionalization of EMFs is an important step in order to serve these practical purposes. Successful derivatization of $La@C_{82}$ by disilacyclopropane under photochemical conditions reported by Akasaka et al.[28] in 1995 pave the way to systematic research devoted to functionalization of different endohedral fullerenes. Currently, a wide range of chemical transformations, such as Diels-Alder (DA) reactions,[29,30] 1,3-dipolar cycloadditions,[31,32] Bingel-Hirsch additions,[33-36] and radical reactions[37,38] are known in which EMFs can be involved.

Ion-encapsulated fullerenes have emerged as a new family of endohedral fullerenes.[39-42] Despite the fact that only lithium-ion-encapsulated C_{60} fullerene ($Li^+@C_{60}$) was isolated and characterized first in 2010,[43] there is a significant number of experimental[44,45] and theoretical[46-48] studies suggesting that the encapsulation of cationic species enhances the reactivity of C_{60} moiety. $Li^+@C_{60}$ also demonstrates the enhanced reactivity in photoinduced electron-transfer reductions compared to pristine C_{60}.[49] Moreover, it forms strong supramolecular complexes with various electron donor systems having long-lived charge-separated states.[49-51] Cycloaddition reactions, in particular, the DA reaction has been extensively utilized for chemical functionalization of fullerenes to produce a variety of fullerene derivatives.[52] The DA reaction rate of $Li^+@C_{60}$ with cyclopentadiene was reported to be 3 order of magnitude faster compared to empty C_{60}.[44] The experimentally measured activation barrier for the DA reaction between 1,3-cyclohexadiene (1,3-CHD) and $Li^+@C_{60}$ was found to be 5.7 kcal/mol lower than that for empty C_{60}. The observed difference was associated with the lowering of the LUMO level of $Li^+@C_{60}$ (-3.74eV) with respect to pristine C_{60} (-2.70eV).[45] For the same reason but in the opposite direction, it has been shown that the incarceration of anions in fullerenes, like in $Cl^-@C_{60}$, decreases the reactivity of the fullerenic cage.[48]

Introduced by the superatom concept numerous stable clusters that mimic the chemical behavior of halogens and alkalis atoms have been discovered.[53-55] In the early 80s Gutsev and Boldyrev have demonstrated the existence of two classes of extraordinary molecular systems – superalkalis (SAs) and superhalogens (SHs).[56,55] SHs are polyatomic systems featured by electron affinities (EAs) that may exceed the limit of chlorine (i.e. 3.61 eV),[56] while SAs are molecules possessing lower ionization potentials (IPs) than this value for cesium (i.e. 3.89 eV).[55] SHs can be used for oxidizing molecules with high ionization potentials, such as benzene or carbon dioxide[57,58] and in the production of organic superconductors.[59] SAs are also of great importance in chemistry since they can exhibit pronounced non-linear optical (NLO) properties.[60] The first SA,

[a] M.Sc. Gibu George, Dr. A. J. Stasyuk, Prof. Dr. M. Solà
Institut de Química Computacional and Departament de Química, Universitat de Girona, C/ Maria Aurèlia Capmany 69, 17003 Girona, Spain.
E-mail:antony.stasuk@gmail.com
E-mail:miquel.sola@udg.edu
[b] Dr. A. J. Stasyuk
Faculty of Chemistry, University of Warsaw, Pasteura 1, 02-093 Warsaw, Poland.
Electronic Supplementary Information (ESI) available: [details of any supplementary information available should be included here]. See DOI: 10.1039/x0xx00000x

OLi_3, was discovered experimentally by Wu et al. in 1979.[61] These systems are found to be thermodynamically stable towards dissociation or loss of an electron.[62] Although different varieties of the species of this kind have been reported,[63,64] several studies have been dedicated to lithium-based superalkalis encapsulated in fullerenes.[65-67]

In this work, we report a mechanistic study of DA reaction involving SA/SH@C_{60} (SA=Li_2F^+, SH=LiF_2^-) species as the dienophile and 1,3-CHD as diene. The main aim is to determine the effect on the reactivity of the fullerenic cage caused by the encapsulated SA or SH. A detailed comparison of the results obtained for SA/SHs and conventional neutral, cationic, and anionic derivatives is used for the rationalization of the effect of encapsulated super atoms on the reactivity of the C_{60} cage. The activation strain model in junction with energy decomposition analysis is used for quantification and understanding the observed effects for such EMFs.

Experimental

Quantum-chemical calculations

Geometry optimization was carried out using the M06-2X hybrid functional[68] equipped with Ahlrichs' Def2-SVP double-ξ quality basis set[69] to explore minimum-energy structures. M06-2X functional was selected due to its high performance towards van der Waals interaction description. Also, it provides good results for the description of pericyclic reactions in endohedral fullerenes.[70,45] The empirical D3 dispersion correction was employed in all cases.[71] The inclusion of Grimme D3 correction increase accuracy of the M06-2X functional towards the description of dispersion complexes. Also it has been shown that inclusion of dispersion corrections is essential for an accurate description of the DA reactions in fullerenes.[72] Normal-mode vibrational frequencies were calculated in each case to confirm the presence of the extremum, at the same level of theory. Thermal corrections to Gibbs energy were calculated at the density functional theory (DFT) level and referred to the gas phase at 1 atm and 298 K. The nature of the transition states was verified using intrinsic reaction coordinate (IRC) calculations[73] to confirm that the corresponding normal mode connects reactants and products. Single-point energy refinements were carried out at M06-2X-D3/def2-TZVPP//M06-2X-D3/def2-SVP level of theory.[68,69] The atomic charge analysis was carried out with the non-iterative ACP scheme.[74]

Activation strain analysis

The activation strain model (ASM)[75], also known as distortion/interaction model, is a fragment-based approach for analyzing and understanding the chemical reactions and to gain insights into the factors that control the heights of the reaction barriers.[76-79] In this model, the energy ΔE(ζ) is decomposed along the reaction coordinate ζ, into activation strain energy $\Delta E_{strain}(\zeta)$, which is the energy associated with the deformation of the reactants from their equilibrium geometry into the geometry that they adopt in the interacting complex along the reaction pathway plus the interaction energy $\Delta E_{int}(\zeta)$, between the deformed reactants:

$$\Delta E(\zeta) = \Delta E_{strain}(\zeta) + \Delta E_{int}(\zeta) \quad (1)$$

Energy decomposition analysis

In the present study of the DA cycloaddition reaction the energy decomposition ΔE(ζ) is carried out along the IRC path on the forming C···C bond between the dienophile (SA/SH@C_{60}) and 1,3-CHD from the initial reactant complex to the transition states. The interaction energy $\Delta E_{int}(\zeta)$ between the deformed reactants was examined in the framework of the Kohn-Sham MO model using a quantitative energy decomposition analysis (EDA)[80-82] into electrostatic interactions, Pauli repulsive orbital interactions, and attractive orbital interactions, to which a term ΔE_{disp} is added to account for the dispersion correction:

$$\Delta E_{int}(\zeta) = \Delta V_{elstat}(\zeta) + \Delta E_{Pauli}(\zeta) + \Delta E_{orb}(\zeta) + \Delta E_{disp}(\zeta) \quad (2)$$

The electrostatic interaction ΔE_{elstat}, which is usually attractive, is the energy between the unperturbed charge distribution of the deformed reactants. The Pauli repulsion term ΔE_{Pauli} is responsible for steric repulsions comprising from the destabilizing interaction between the occupied orbitals of the reactant fragments. The orbital interaction term ΔE_{orb}, accounts for the charge transfer between the occupied orbitals of one moiety and unoccupied orbitals of another moiety and the polarization due to the mixing of empty and occupied orbitals within each reactant species. Lastly, the dispersion term ΔE_{disp}, accounts for the interactions due to dispersion forces.[83] The EDA calculations were carried out at B3LYP-D3/TZ2P level on M06-2X/def2-SVP optimized geometries as implemented in Amsterdam Modeling Suit package.[84]

Results and discussion

Considering that the size of C_{60} cavity is rather big compared to Li_2F^+, and LiF_2^- ions it seems likely that their rotation will be unconstrained. This in turn means that if there are several conformers with different relative fragment orientations with respect to each other, then they should be practically isoenergetic. For verification of this hypothesis, we generated 26 starting geometries for SA/SH@C_{60} systems different in terms of the orientation of Li_2F^+, and LiF_2^- fragments (Fig. S1, SI). An optimization procedure revealed that energies of obtained structures differ from each other by an amount not exceeding 1 kcal/mol. Thus, we can assert that the rotation of the encapsulated SA/SH fragments inside the C_{60} cage is free.

The cycloaddition reactions involving C_{60} fullerene species, as it was demonstrated earlier, favors [6,6] over [5,6] bonds due to the stronger or effective overlap between the orbitals of the reactants throughout the reaction coordinate.[85] Thus, at the initial stage we have explored the DA reaction between 1,3-CHD

with SA/SH@C_{60} by focusing on the reaction involving [6,6]-pyracylenic bond of the C_{60} cage. The reaction proceeds through a preformed initial reactant complex (RC) towards the product or cycloadduct (CA) via a transition state (TS, see Figure 1) Structures of other complexes are provided in Figure S2, SI

.

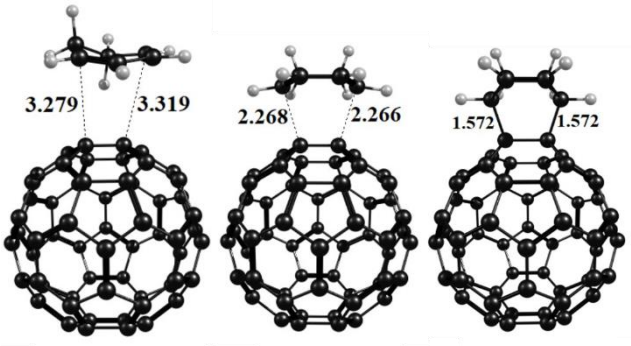

Figure 1. Structures of the RC, TS, and CA involved in the DA reaction between 1,3-CHD and C_{60} fullerene were obtained at M06-2X-D3/def2-SVP level of theory. Highlighted formed bond lengths are given in angstroms.

The computed reaction energy profile for [4+2] cycloaddition reaction between 1,3-CHD and SA/SH@C_{60} or empty C_{60} species is presented on Figure 2. As seen the activation energy barrier (ΔE_a) for empty C_{60} and LiF_2^-@C_{60} complexes is significantly higher compared to that for reactions involving Li_2F^+ (ΔE_a = 17.9 > 17.6 > 13.2 kcal/mol for empty C_{60}, LiF_2^-@C_{60}, and Li_2F^+@C_{60} species respectively).

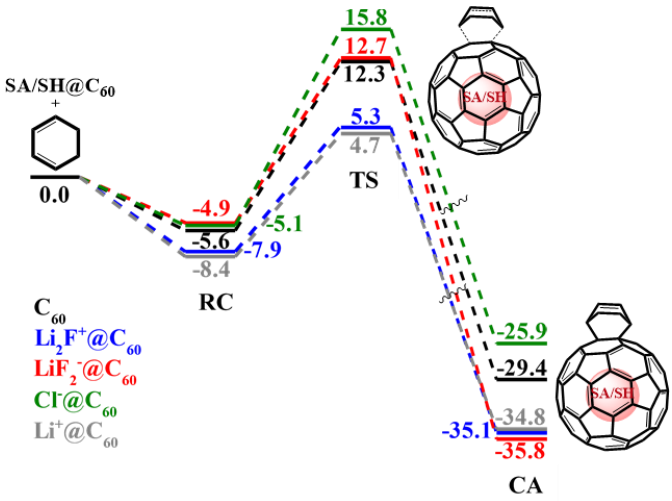

Figure 2. Computed reaction profile for Diels-Alder reaction between 1,3-CHD and C_{60} fullerene with encapsulated cationic/anionic species. All the data were computed at the M06-2X-D3/def2-TZVPP//M06-2X-D3/def2-SVP level of theory. Relative energies are given in kcal/mol.

The computed energy barrier for C_{60} fullerene is in good agreement with the experimentally measured values (17.9 vs 16.8 kcal/mol respectively).[45] Moreover, the reduction of the energy barrier by 4.7 kcal/mol due to Li^+ encapsulation is close to the 5.7 kcal/mol found experimentally.[45] All these results confirm the adequacy of the selected level of theory. We have noticed that complexes based on superalkali cation (Li_2F^+@C_{60}) behave very similar to the one based on Li^+ cationic species (Li^+@C_{60}). Incorporation into the fullerene cage of both superalkaline and superhalogen species makes the DA reaction more thermodynamically favorable compared to the empty C_{60} (ΔE_R = -29.4 < -35.1 < -35.8 kcal/mol for empty C_{60}, Li_2F^+@C_{60}, and LiF_2^-@C_{60} respectively). Important to note that cationic Li^+ and Li_2F^+ species substantially decrease activation barrier makes the reaction more favorable kinetically, while anionic Cl^- and LiF_2^- species slightly increase reaction barrier compared to parental C_{60}.

To get more insight into the reactivities of considered SA/SH encapsulated fullerenes, we have performed a detailed study of the DA cycloaddition reactions using the activation strain model (ASM). Figure 3 shows the activation-strain diagrams for the cycloaddition reactions between 1,3-CHD and C_{60} (solid lines), Li_2F^+@C_{60} (dotted lines), and LiF_2^-@C_{60} (dashed lines) from the reactant complexes to the corresponding transition states. The shape of the different curves is rather similar, which is typical for other types of pericyclic reactions.[86] In particular, for all systems the strain energy ΔE_{strain} monotonically increases along with the reaction coordinate, whereas the interaction energy ΔE_{int} between the deformed reactants only becomes more stabilizing while approaching the transition-state region. As seen from Figure 3, the difference in the total energy change is mainly derived from the interaction energy and not from the strain energy. Thus, the interaction energy between the deformed reactants becomes the decisive factor responsible for the observed reactivity trend.

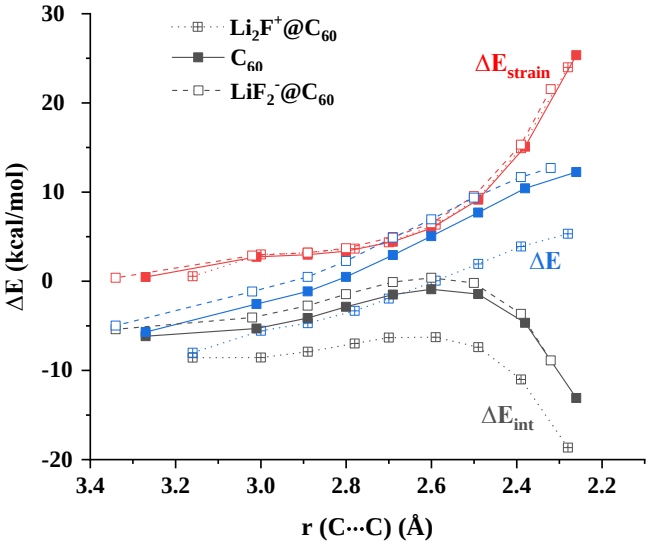

Figure 3. Activation strain diagrams of the Diels-Alder reaction between 1,3-CHD and C_{60} (solid lines), Li_2F^+@C_{60} (dotted lines), and LiF_2^-@C_{60} (dashed lines) along the intrinsic reaction coordinate projected onto the forming C···C bond length. The energies were computed at M06-2X-D3/def2-TZVPP//M06-2X-D3/def2-SVP level of theory.

The reaction involving Li_2F^+@C_{60} exhibits a much smaller total energy change ΔE compared to empty C_{60} and LiF_2^-@C_{60} along the IRC path from the RC to TS. This leads to the lower activation barrier for DA reaction between Li_2F^+@C_{60} and 1,3-CHD. The difference in this total energy change is mainly derived from the interaction energy and not from the strain energy. The shape of the curve for the deformation energy is very much

similar for all the systems such that the strain energy ΔE_{strain} steadily increases along the reaction path. Conversely, the interaction energy ΔE_{int} tends to be stabilizing upon reaching the transition state. This is an indication that the interaction energy between the deformed reactants becomes the decisive factor responsible for the observed reactivity trend. It can be illustrated by a comparison of the difference in the interaction energy ($\Delta\Delta E_{int}$) of reactions involving $Li_2F^+@C_{60}$ *vs.* C_{60} and $Li_2F^+@C_{60}$ *vs.* $LiF_2^-@C_{60}$ at the same forming C···C distance of 2.4 Å ($\Delta\Delta E_{int}$ = 6.4 and 7.4 kcal/mol respectively). As seen these values roughly match the computed total energy difference between the same transformations (ΔΔE = 6.5 and 7.8 kcal/mol respectively). The energies calculated using ASM along the IRC path for the Diels-Alder reaction involving $Li_2F^+@C_{60}$, empty C_{60}, and $LiF_2^-@C_{60}$ are given in the Table S1, S2, and S3, SI respectively. Note that the behavior of Li^+ encapsulated system is very similar to that of its SA analog. Therefore, it can be concluded that the presence of Li_2F^+ cation inside the C_{60} enhances the DA reactivity as compared to empty C_{60}. The reaction became more kinetically favorable as a consequence of a significantly stronger interaction between the reactants from the initially formed reactant complex up to the corresponding transition state. In contrast, as reported for Cl^-,[48] the presence of LiF_2^- anion has the opposite effect - the interaction energies in the case of encapsulated anionic species became weaker than in the process involving the parent C_{60} and therefore increases in the activation energy of the DA reaction.

Energy decomposition analysis (EDA) has been performed to get a deeper understanding of the different contributors to the total interaction energy between the deformed reactants. Figure 4 illustrates the EDA terms for the reaction involving C_{60} (solid lines), $Li_2F^+@C_{60}$ (dotted lines), and $LiF_2^-@C_{60}$ (dashed lines).

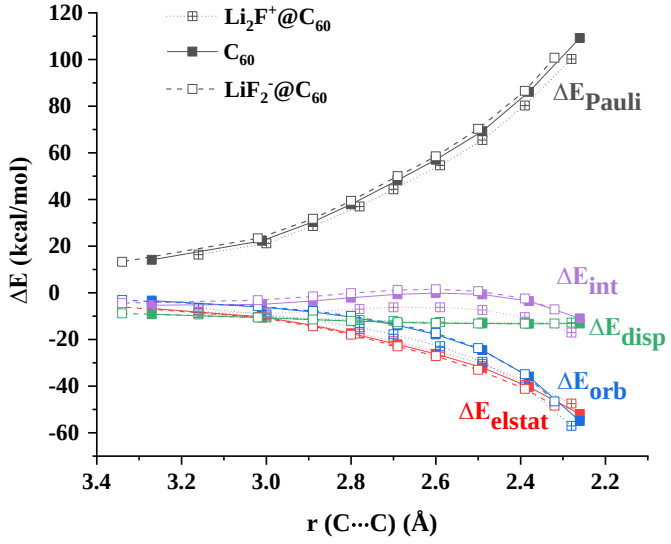

Figure 4. Energy decomposition of the interaction energy for the Diels-Alder reaction between 1,3-CHD and C_{60} (solid lines), $Li_2F^+@C60$ (dotted lines), and $LiF_2^-@C60$ (dashed lines) along the intrinsic reaction coordinate projected onto the forming C···C bond length. The energies were computed at B3LYP-D3/TZ2P//M06-2X-D3/def2-SVP level of theory.

The larger interaction energy observed for the $Li_2F^+@C_{60}$ system is solely from the stronger orbital interaction between the reactants along the reaction coordinate. For instance, the order of orbital interaction energy ΔE_{orb}, at the same forming C···C distance of 2.4 Å is -40.2 ($Li_2F^+@C_{60}$) > -36.0 (C_{60}) > -34.8 kcal/mol ($LiF_2^-@C_{60}$). The superalkali cationic system is also favored by a slightly smaller destabilizing Pauli repulsion term ΔE_{Pauli} compared to the other two systems (ΔE_{Pauli} = 80.3 ($Li_2F^+@C_{60}$) < 86.1 (C_{60}) < 86.7 kcal/mol ($LiF_2^-@C_{60}$)). The increase in Pauli repulsion term from $Li_2F^+@C_{60}$ to $LiF_2^-@C_{60}$ systems is due to the fact that anion encapsulation leads to a significant gain in electron density for the carbon atoms of C_{60} cage.[87] Detailed EDA results with the percentage contributions to the sum of all attractive energy terms for the systems

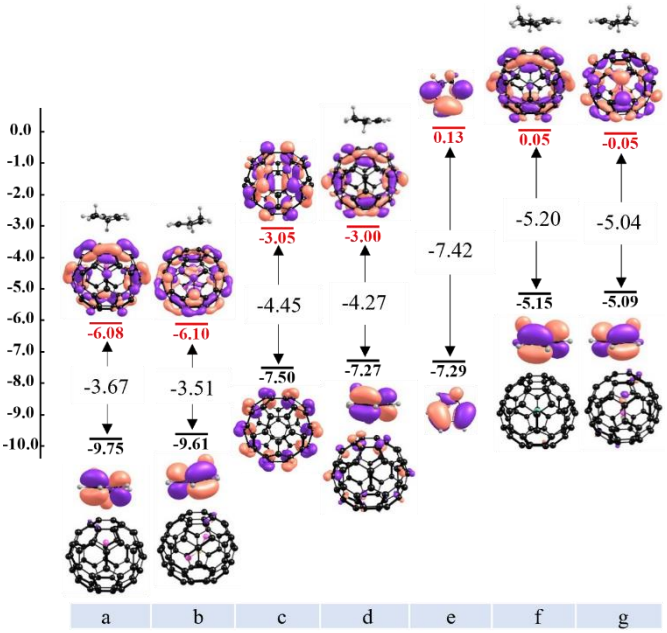

Figure 5. Frontier HOMO and LUMO of (a) RC-$Li^+@C60$, (b) RC-$Li_2F^+@C_{60}$, (c) isolated C_{60}, (d) RC-C_{60}, (e) isolated 1,3-CHD, (f) RC-$Cl^-@C_{60}$, (g) RC-$LiF_2^-@C_{60}$ with energies in eV computed at M06-2X-D3/def2-TZVPP//M06-2X-D3/def2-SVP level of theory. Orbitals are drawn on the isodensity surface of 0.03 e/Å.

corresponding to $Li_2F^+@C_{60}$, empty C_{60}, and $LiF_2^-@C_{60}$ are provided in the Table S4, S5, and S6, SI respectively.

The difference in the orbital interaction energy between SA/SH@C_{60} and empty C_{60} systems can be explained considering the molecular orbitals involved in these interactions. Figure 5 shows the calculated frontier HOMO-LUMO energies of the studied complexes.

As seen in Figure 5, energies of the frontier HOMO and LUMO of neutral and charged complexes differ significantly. In the neutral complex in RC geometry, HOMO is localized on 1,3-CHD, while LUMO is localized on C_{60} fullerene. As it has been shown in a previous study, the HOMO(diene)-LUMO(C_{60}) is the most frontier MO relevant interaction.[48] Their energies are similar to that of the isolated fragments: -7.27 vs -7.29 eV for 1,3-CHD in complex and isolated form, and -3.00 vs -3.05 eV for C_{60} in complex and isolated form respectively. The HOMO-

LUMO gap (HL gap) in the case of the neutral system was found to be 4.27 eV. Incorporation of the Li^+/Li_2F^+ cations into the C_{60} cage leads to sharp changes in the orbital energy. The energy of LUMO stabilized by about 3 eV, stabilization of HOMO is slightly less and amounts to 2.3-2.5 eV. These changes in turn lead to the reduction of the HL gap to 3.51 and 3.67 eV for $Li_2F^+@C_{60}$ and $Li^+@C_{60}$ complexes respectively. In turn, Cl^-/LiF_2^- anions incorporated in the cage lead to destabilization of HOMO and LUMO energies, while the HL gap increases to more than 5 eV (Figure 5). Interestingly to note that the effect of the included SA and SH species on the HL gap has almost the same magnitude, but the opposite direction. Observed changes are caused by the electrostatic effect of the charged species incorporated into the cage. The electrostatic effect of the charged species that 1,3-CHD experience in the RC are less than for C_{60} due to the larger effective distance. A smaller HL gap observed for $Li_2F^+@C_{60}$ compared to other studied complexes describes the decisive role of orbital interaction and this also attributes to the lower activation barrier. Frontier HOMO-LUMO for the TS geometry of the studied complexes are provided in Figure S3, SI.

At the next stage, we have compared the stability of the reaction complexes and cycloadduct products for studied systems (Figure 2). The $Li_2F^+@C_{60}$ and $Li^+@C_{60}$ demonstrate very similar behavior. The relative energies of RC, CA, and TS structures for both cation encapsulated complexes are almost identical and do not exceed 0.6 kcal/mol. Our attention was drawn by unusual stability for the TS and CA structures of $LiF_2^-@C_{60}$ in contrast to the $Cl^-@C_{60}$ complex. The Diels-Alder reaction involving $LiF_2^-@C_{60}$ was found to be a significantly more favorable compared to $Cl^-@C_{60}$ both kinetically (ΔE_a = 20.9 > 17.6 kcal/mol for $Cl^-@C_{60}$ and $LiF_2^-@C_{60}$, respectively) and thermodynamically (ΔE_R = -25.9 < -35.4 kcal/mol for $Cl^-@C_{60}$ and $LiF_2^-@C_{60}$, respectively). To understand the nature of the observed cycloadduct stabilities the interaction energy (ΔE_{int}) between 1,3-CHD and ion-encapsulated C_{60} and empty C_{60} was computed.

Table 1. Interaction (ΔE_{int}), deformation (ΔE_{def}), and total energies (ΔE) for cycloadducts in the DA reaction between diene (1,3-CHD) and $X@C_{60}$ species, where X = empty C_{60}, Li^+, Li_2F^+, Cl^-, LiF_2^-.[a,b]

X@C60···1,3-CHD	ΔEint	ΔEdef			ΔE
		1,3-CHD	C60	total	
C60	-175.06	100.24	45.42	145.65	-29.41
Li+@C60	-181.11	99.76	46.52	146.28	-34.83
Li2F+@C60	-181.33	99.79	46.47	146.27	-35.06
Cl-@C60	-170.65	100.51	44.25	144.75	-25.90
LiF2-@C60	-179.06	101.23	42.05	143.28	-35.77

[a] The energy values are in kcal/mol. [b] Energies obtained at M06-2X-D3/def2-TZVPP//M06-2X-D3/def2-SVP level of theory.

The interaction energy decreases in the order $Li_2F^+@C_{60}$ > $Li^+@C_{60}$ > $LiF_2^-@C_{60}$ > empty C_{60} > $Cl^-@C_{60}$. As seen the ΔE_{int} for $Li^+/Li_2F^+@C_{60}$ is higher than for $LiF_2^-@C_{60}$ by about 2 kcal/mol. However, $LiF_2^-@C_{60}$ complex is slightly more stable compared to $Li_2F^+@C_{60}$ due to its lower strain energy (Table 1). The smaller deformation energy for the $LiF_2^-@C_{60}$ system is associated with the smaller deformation energy of the fullerene unit.

The interaction and deformation energies between 1,3-CHD and anion-encapsulated systems in their TS geometries were computed to explain smaller activation energy for $LiF_2^-@C_{60}$ compared to the $Cl^-@C_{60}$ complex.

Table 2. Interaction (ΔE_{int}), deformation (ΔE_{def}), and total energies (ΔE), as well as ACP charges computed for TS structures in the DA reaction between diene (1,3-CHD) and $Cl^-/LiF_2^-@C_{60}$ endohedral complexes.[a,b]

Complex	ΔEint	ΔEdef			Charges			ΔE
		1,3-CHD	Cage	Total	1,3-CHD	C60	Encapsulated species	
Cl-@C60	-10.48	5.72	20.58	26.29	-0.01	-0.30	-0.67	15.82
LiF2-@C60	-8.85	4.15	17.42	21.58	-0.02	-0.04	-0.93	12.72

[a] The energy values are in kcal/mol. [b] Energies obtained at M06-2X-D3/def2-TZVPP//M06-2X-D3/def2-SVP level of theory.

As seen from Table 2, the $Cl^-@C_{60}$ complex is characterized by slightly stronger interaction energy between the fullerene cage and 1,3-CHD unit compared to $LiF_2^-@C_{60}$. However, differences in interaction energies between these two complexes are only 1.6 kcal/mol. At the same time for $Cl^-@C_{60}$ deformation energies by 4.7 kcal/mol higher. It is important to note that the main contributor to this difference is fullerene. These findings seem counterintuitive given the markedly larger size of LiF_2^- anion compared to Cl^-. In order to explain this observation, we have computed charges on 1,3-CHD, fullerene, and encapsulated units in both complexes (Table 2). In the case of $LiF_2^-@C_{60}$, the negative charge is almost completely localized on LiF_2^- anion, while in $Cl^-@C_{60}$ complex it is partially shifted from Cl^- to the C_{60} cage. This can be explained by considering the fact that the electron affinity of LiF_2 is significantly higher than that for Cl (4.32 eV vs 3.36 eV for LiF_2 and Cl respectively). Thus, the excess of the electron density on the C_{60} leads to its higher reorganization energy in $Cl^-@C_{60}$ as compared to $LiF_2^-@C_{60}$ in the TS and the CA.

Conclusions

In summary, the Diels-Alder cycloaddition reaction between 1,3-CHD and endohedral C_{60} fullerenes with encapsulated (super)alkali/(super)halogen species has been studied by DFT method. A significant enhancement in reactivity was observed for the systems with encapsulated Li^+/Li_2F^+ cations. The ASM-EDA analysis confirms that the interaction energy between the

reactants plays a crucial role in the kinetic stability of the $Li_2F^+@C_{60}$. Its strong interaction energy is associated with the enhanced orbital interactions between cyclohexadiene and $Li_2F^+@C_{60}$. In the case of encapsulation by C_{60} of superhalogen anion LiF_2^-, the cycloadduct was found to be the most thermodynamically preferred among the rest of products, whereas in the case of Cl^- anion the cycloaddition reaction becomes unfavorable both kinetically and thermodynamically. According to the ASM analysis, lower stability of the reaction product and higher activation energy barrier for $Cl^-@C_{60}$ in comparison to the other studied complexes are caused by small interaction energy between the reactants and high deformation energy of $Cl^-@C_{60}$ cage.

Conflicts of interest

There are no conflicts to declare.

Acknowledgements

We are grateful for financial support from the Spanish Ministerio de Ciencia e Innovación (Network RED2018-102815-T, project PID2020-113711GB-I00, and Juan de la Cierva contracts IJC2019-039846-I to A.J.S.) and the Catalan Conselleria de Recerca i Universitats (project 2017SGR39 and contract 2020 FISDU 00345 to G.G.). We are also thankful for the computational time financed by the Consorci de Serveis Universitaris de Catalunya (CSUC).

References

1 J. R. Heath, S. C. O'Brien, Q. Zhang, Y. Liu, R. F. Curl, F. K. Tittel and R. E. Smalley, *J. Am. Chem. Soc.*, 1985, **107**, 7779–7780.
2 N. Martín, *Chem. Commun.*, 2006, 2093–2104.
3 M. N. Chaur, F. Melin, A. L. Ortiz and L. Echegoyen, *Angew. Chemie Int. Ed.*, 2009, **48**, 7514–7538.
4 M. Yamada, T. Akasaka and S. Nagase, *Acc. Chem. Res.*, 2010, **43**, 92–102.
5 A. A. Popov, S. Yang and L. Dunsch, *Chem. Rev.*, 2013, **113**, 5989–6113.
6 D. S. Bethune, R. D. Johnson, J. R. Salem, M. S. de Vries and C. S. Yannoni, *Nature*, 1993, **366**, 123–128.
7 S. Yang, T. Wei and F. Jin, *Chem. Soc. Rev.*, 2017, **46**, 5005–5058.
8 X. Lu, L. Feng, T. Akasaka and S. Nagase, *Chem. Soc. Rev.*, 2012, **41**, 7723–7760.
9 R. Tellgmann, N. Krawez, S.-H. Lin, I. V Hertel and E. E. B. Campbell, *Nature*, 1996, **382**, 407–408.
10 E. E. B. Campbell, R. Tellgmann, N. Krawez and I. V Hertel, *J. Phys. Chem. Solids*, 1997, **58**, 1763–1769.
11 Y. Kubozono, H. Maeda, Y. Takabayashi, K. Hiraoka, T. Nakai, S. Kashino, S. Emura, S. Ukita and T. Sogabe, *J. Am. Chem. Soc.*, 1996, **118**, 6998–6999.
12 E. Nishibori, M. Takata, M. Sakata, M. Inakuma and H. Shinohara, *Chem. Phys. Lett.*, 1998, **298**, 79–84.
13 Y. Rubin, *Chem. – A Eur. J.*, 1997, **3**, 1009–1016.
14 E. G. Gillan, C. Yeretzian, K. S. Min, M. M. Alvarez, R. L. Whetten and R. B. Kaner, *J. Phys. Chem.*, 1992, **96**, 6869–6871.
15 K. Kurotobi and Y. Murata, *Science (80-.).*, 2011, **333**, 613 LP – 616.
16 K. Komatsu, M. Murata and Y. Murata, *Science (80-.).*, 2005, **307**, 238 LP – 240.
17 A. Krachmalnicoff, R. Bounds, S. Mamone, S. Alom, M. Concistrè, B. Meier, K. Kouřil, M. E. Light, M. R. Johnson, S. Rols, A. J. Horsewill, A. Shugai, U. Nagel, T. Rõõm, M. Carravetta, M. H. Levitt and R. J. Whitby, *Nat. Chem.*, 2016, **8**, 953–957.
18 L. Dunsch and S. Yang, *Phys. Chem. Chem. Phys.*, 2007, **9**, 3067–3081.
19 S. Yang, A. A. Popov and L. Dunsch, *Angew. Chemie Int. Ed.*, 2007, **46**, 1256–1259.
20 E. E. Maroto, J. Mateos, M. Garcia-Borràs, S. Osuna, S. Filippone, M. Á. Herranz, Y. Murata, M. Solà and N. Martín, *J. Am. Chem. Soc.*, 2015, **137**, 1190–1197.
21 S. Vidal, M. Izquierdo, S. Alom, M. Garcia-Borràs, S. Filippone, S. Osuna, M. Solà, R. J. Whitby and N. Martín, *Chem. Commun.*, 2017, **53**, 10993–10996.
22 T. Da Ros and M. Prato, *Chem. Commun.*, 1999, 663–669.
23 J.-F. Nierengarten, J.-F. Eckert, D. Felder, J.-F. Nicoud, N. Armaroli, G. Marconi, V. Vicinelli, C. Boudon, J.-P. Gisselbrecht, M. Gross, G. Hadziioannou, V. Krasnikov, L. Ouali, L. Echegoyen and S.-G. Liu, *Carbon N. Y.*, 2000, **38**, 1587–1598.
24 E. Castro, A. H. Garcia, G. Zavala and L. Echegoyen, *J. Mater. Chem. B*, 2017, **5**, 6523–6535.
25 E. I. Pochkaeva, N. E. Podolsky, D. N. Zakusilo, A. V Petrov, N. A. Charykov, T. D. Vlasov, A. V Penkova, L. V Vasina, I. V Murin, V. V Sharoyko and K. N. Semenov, *Prog. Solid State Chem.*, 2020, **57**, 100255.
26 L. Jia, M. Chen and S. Yang, *Mater. Chem. Front.*, 2020, **4**, 2256–2282.
27 T. Akasaka and S. Nagase, *Endofullerenes: a new family of carbon clusters*, Springer Science & Business Media, 2002, vol. 3.
28 T. Akasaka, T. Kato, K. Kobayashi, S. Nagase, K. Yamamoto, H. Funasaka and T. Takahashi, *Nature*, 1995, **374**, 600–601.
29 S. Osuna, M. Swart, J. M. Campanera, J. M. Poblet and M. Solà, *J. Am. Chem. Soc.*, 2008, **130**, 6206–6214.
30 S. Osuna, M. Swart and M. Solà, *J. Am. Chem. Soc.*, 2009, **131**, 129–139.
31 M. Maggini, G. Scorrano and M. Prato, *J. Am. Chem. Soc.*, 1993, **115**, 9798–9799.
32 M. Prato and M. Maggini, *Acc. Chem. Res.*, 1998, **31**, 519–526.
33 C. Bingel, *Chem. Ber.*, 1993, **126**, 1957–1959.
34 P. Besalú-Sala, J. M. Luis and M. Solà, *Chem. - A Eur. J.*, 2020, **26**, 14481–14487.
35 J. P. Martínez, M. Garcia-Borràs, S. Osuna, J. Poater, F. M. Bickelhaupt and M. Solà, *Chem. – A Eur. J.*, 2016, **22**, 5953–5962.
36 M. Garcia-Borràs, M. R. Cerón, S. Osuna, M. Izquierdo, J. M. Luis, L. Echegoyen and M. Solà, *Angew. Chemie Int. Ed.*, 2016, **55**, 2374–2377.
37 H. Nikawa, T. Kikuchi, T. Wakahara, T. Nakahodo, T. Tsuchiya, G. M. A. Rahman, T. Akasaka, Y. Maeda, K. Yoza, E. Horn, K. Yamamoto, N. Mizorogi and S. Nagase, *J. Am. Chem. Soc.*, 2005, **127**, 9684–9685.
38 X. Lu, L. Bao, T. Akasaka and S. Nagase, *Chem. Commun.*, 2014, **50**, 14701–14715.
39 H. Ueno, K. Kokubo, Y. Nakamura, K. Ohkubo, N. Ikuma, H. Moriyama, S. Fukuzumi and T. Oshima, *Chem. Commun.*, 2013, **49**, 7376–7378.
40 S. Fukuzumi, K. Ohkubo, Y. Kawashima, D. S. Kim, J. S. Park, A. Jana, V. M. Lynch, D. Kim and J. L. Sessler, *J. Am. Chem. Soc.*, 2011, **133**, 15938–15941.
41 S. Aoyagi, Y. Sado, E. Nishibori, H. Sawa, H. Okada, H. Tobita, Y. Kasama, R. Kitaura and H. Shinohara, *Angew. Chemie Int. Ed.*, 2012, **51**, 3377–3381.

42 H. Okada, T. Komuro, T. Sakai, Y. Matsuo, Y. Ono, K. Omote, K. Yokoo, K. Kawachi, Y. Kasama, S. Ono, R. Hatakeyama, T. Kaneko and H. Tobita, *RSC Adv.*, 2012, **2**, 10624–10631.
43 S. Aoyagi, E. Nishibori, H. Sawa, K. Sugimoto, M. Takata, Y. Miyata, R. Kitaura, H. Shinohara, H. Okada, T. Sakai, Y. Ono, K. Kawachi, K. Yokoo, S. Ono, K. Omote, Y. Kasama, S. Ishikawa, T. Komuro and H. Tobita, *Nat. Chem.*, 2010, **2**, 678–683.
44 H. Kawakami, H. Okada and Y. Matsuo, *Org. Lett.*, 2013, **15**, 4466–4469.
45 H. Ueno, H. Kawakami, K. Nakagawa, H. Okada, N. Ikuma, S. Aoyagi, K. Kokubo, Y. Matsuo and T. Oshima, *J. Am. Chem. Soc.*, 2014, **136**, 11162–11167.
46 C.-X. Cui and Y.-J. Liu, *J. Phys. Chem. A*, 2015, **119**, 3098–3106.
47 J. Karimi, M. Izadyar and A. Nakhaeipour, *Struct. Chem.*, 2020, **31**, 1821–1829.
48 Y. García-Rodeja, M. Solà, F. M. Bickelhaupt and I. Fernández, *Chem. - A Eur. J.*, 2017, **23**, 11030–11036.
49 Y. Kawashima, K. Ohkubo and S. Fukuzumi, *Chem. – An Asian J.*, 2015, **10**, 44–54.
50 H. Ueno, T. Nishihara, Y. Segawa and K. Itami, *Angew. Chemie Int. Ed.*, 2015, **54**, 3707–3711.
51 A. J. Stasyuk, O. A. Stasyuk, M. Solà and A. A. Voityuk, *Chem. Commun.*, 2019, **55**, 11195–11198.
52 G. H. Sarova and M. N. Berberan-Santos, *Chem. Phys. Lett.*, 2004, **397**, 402–407.
53 X.-B. Wang, C.-F. Ding, L.-S. Wang, A. I. Boldyrev and J. Simons, *J. Chem. Phys.*, 1999, **110**, 4763–4771.
54 G. L. Gutsev and A. I. Boldyrev, *Chem. Phys.*, 1981, **56**, 277–283.
55 G. L. Gutsev and A. I. Boldyrev, *Chem. Phys. Lett.*, 1982, **92**, 262–266.
56 G. L. Gutsev and A. I. Boldyrev, *Chem. Phys. Lett.*, 1981, **84**, 352–355.
57 M. Czapla, S. Freza and P. Skurski, *Chem. Phys. Lett.*, 2015, **619**, 32–35.
58 M. Czapla and P. Skurski, *Phys. Chem. Chem. Phys.*, 2017, **19**, 5435–5440.
59 F. Wudl, *Acc. Chem. Res.*, 1984, **17**, 227–232.
60 J. Mai, S. Gong, N. Li, Q. Luo and Z. Li, *Phys. Chem. Chem. Phys.*, 2015, **17**, 28754–28764.
61 C. H. Wu, H. Kudoa) and H. R. Ihle, *J. Chem. Phys.*, 1979, **70**, 1815–1820.
62 P. v. R. Schleyer, E. U. Wuerthwein and J. A. Pople, *J. Am. Chem. Soc.*, 1982, **104**, 5839–5841.
63 E. Rehm, A. I. Boldyrev and P. v R. Schleyer, *Inorg. Chem.*, 1992, **31**, 4834–4842.
64 J. Tong, Z. Wu, Y. Li and D. Wu, *Dalt. Trans.*, 2013, **42**, 577–584.
65 A. K. Srivastava, A. Kumar and N. Misra, *Chem. Phys. Lett.*, 2017, **682**, 20–25.
66 A. K. Srivastava, S. K. Pandey and N. Misra, *Chem. Phys. Lett.*, 2016, **655**–**656**, 71–75.
67 G. Meloni, A. Giustini and H. Park, *Front. Chem.*, 2021, **9**, 539.
68 Y. Zhao and D. G. Truhlar, *Theor. Chem. Acc.*, 2008, **120**, 215–241.
69 F. Weigend and R. Ahlrichs, *Phys. Chem. Chem. Phys.*, 2005, **7**, 3297–3305.
70 Y. Wu, Y. Jiang, J. Deng and Z. Wang, *Phys. Chem. Chem. Phys.*, 2020, **22**, 24249–24256.
71 S. Grimme, J. Antony, S. Ehrlich and H. Krieg, *J. Chem. Phys.*, 2010, **132**, 154104.
72 S. Osuna, M. Swart and M. Solà, *J. Phys. Chem. A*, 2011, **115**, 3491–3496.
73 K. Fukui, *Acc. Chem. Res.*, 1981, **14**, 363–368.
74 A. A. Voityuk, A. J. Stasyuk and S. F. Vyboishchikov, *Phys. Chem. Chem. Phys.*, 2018, **20**, 23328–23337.
75 I. Fernández, *Eur. J. Org. Chem.*, 2018, **2018**, 1394–1402.
76 F. M. Bickelhaupt and K. N. Houk, *Angew. Chem. Int. Ed.*, 2017, **56**, 10070–10086.
77 W.-J. van Zeist and F. M. Bickelhaupt, *Org. Biomol. Chem.*, 2010, **8**, 3118–3127.
78 I. Fernández and F. M. Bickelhaupt, *Chem. Soc. Rev.*, 2014, **43**, 4953–4967.
79 L. P. Wolters and F. M. Bickelhaupt, *WIREs Comput. Mol. Sci.*, 2015, **5**, 324–343.
80 K. Morokuma, *J. Chem. Phys.*, 1971, **55**, 1236–1244.
81 K. Kitaura and K. Morokuma, *Int. J. Quantum Chem.*, 1976, **10**, 325–340.
82 T. Ziegler and A. Rauk, *Theor. Chim. Acta*, 1977, **46**, 1–10.
83 F. M. Bickelhaupt and E. J. Baerends, *Rev. Comput. Chem.*, 2000, 1–86.
84 G. te Velde, F. M. Bickelhaupt, E. J. Baerends, C. Fonseca Guerra, S. J. A. van Gisbergen, J. G. Snijders and T. Ziegler, *J. Comput. Chem.*, 2001, **22**, 931–967.
85 I. Fernández, M. Solà and F. M. Bickelhaupt, *Chem. Eur. J.*, 2013, **19**, 7416–7422.
86 I. Fernández, *Phys. Chem. Chem. Phys.*, 2014, **16**, 7662–7671.
87 T. Davis Della and C. H. Suresh, *Phys. Chem. Chem. Phys.*, 2018, **20**, 24885–24893.